Nano Energy 78 (2020) 105261

Contents lists available at ScienceDirect

Nano Energy

journal homepage: www.elsevier.com/locate/nanoen

Full paper

High-temperature silicon thermal diode and switch

Maciej Kasprzak [a,1], Marianna Sledzinska [b,1], Karol Zaleski [c], Igor Iatsunskyi [c], Francesc Alzina [b], Sebastian Volz [d], Clivia M. Sotomayor Torres [b,e], Bartlomiej Graczykowski [a,f,*]

[a] Faculty of Physics, Adam Mickiewicz University, Uniwersytetu Poznanskiego 2, 61-614 Poznan, Poland
[b] Catalan Institute of Nanoscience and Nanotechnology (ICN2), CSIC and BIST, Campus UAB, Bellaterra, 08193, Barcelona, Spain
[c] NanoBioMedical Centre, Adam Mickiewicz University, Wszechnicy Piastowskiej 3, 61-614, Poznan, Poland
[d] LIMMS/CNRS-IIS(UMI2820) Institute of Industrial Science, University of Tokyo 4-6-1 Komaba, Meguro-ku, 153-8505 Tokyo, Japan
[e] ICREA, PG. Lluis Companys 23, 08010, Barcelona, Spain
[f] Max Planck Institute for Polymer Research, Ackermannweg 10, 55128, Mainz, Germany

ARTICLE INFO

Keywords:
Thermal rectification
Thermal switch
Raman thermometry
Thermal diode
High temperatures
Thermoelectrics

ABSTRACT

A thermal rectifier/diode is a nonreciprocal element or system that enables preferential heat transport in one direction. In this work we demonstrate a single-material thermal diode operating at high temperatures. The diode is made of nanostructured silicon membranes exhibiting spatially and temperature-dependent thermal conductivity and, therefore, falling into the category of spatially asymmetric, nonlinear nonreciprocal systems. We used an all-optical state-of-the-art experimental technique to prove rectification along rigorous criteria of the phenomenon. Using sub-milliwatt power we achieve rectification of about 14%. In addition, we demonstrate air-triggered thermal switching and passive cooling. Our findings provide a CMOS-compatible platform for heat rectification and applications in energy harvesting, thermal insulation and cooling, as well as sensing and potentially thermal logic.

1. Introduction

Given the numerous heat-associated challenges currently facing humanity, ranging from global warming to the future of technological miniaturization, there is pressing need for solutions to control the direction of thermal flow. This issue becomes even more important for the processes performed at temperatures ranging from room temperature to hundreds of Kelvin. In particular, it covers mild temperatures dedicated to standard commercial devices, intermediate temperatures typical for the automotive, aircraft engines and conventional energy production up to extreme temperature conditions facing the space exploration or metallurgy [1,2]. Needless to say, high temperature is a huge value market for thermal sensing, energy harvesting and cooling applications. In this regard, despite the wealth of new materials, silicon and silicon on insulator (SOI) technologies remain most mature for production of miniaturized and robust devices operating in high temperature environments [3].

A potential game changer for thermal management is the solid-state thermal rectifier/diode breaking reciprocity in heat flow [4–9]. To date, several micro- and nano-scale thermal diodes using phonon heat conduction rectification have been proposed, which are based on nonlinear media together with a spatial asymmetry of the system [4,10–18]. Despite its good performance, the few real devices presented so far operate below room temperature or require advanced multi-component fabrication [19–22]. In some cases, the claim of true rectification has been questioned from the argument of existing misconceptions in delimiting the system and the improper symmetry of the experiment [5,7,23–26]. Finally, the demonstration of thermal rectification in miniaturized systems biased with temperature gradients exceeding hundreds of Kelvin remains an experimental challenge.

In this work we demonstrate a thermal rectifier made of a single-material, i.e. a holey crystalline silicon membrane operating at high temperature biases. The working principle is similar to some previous theoretical proposals [16,27,28], i.e. single component materials with temperature dependence (non-linearity) and space dependence (spatial asymmetry) of the thermal conductivity. In this case, and contrary to the bi-segmented Si medium of Ref. [22], the system is designed with a continuous variation of the thermal property. The graded structure prevents interface thermal resistance, which is a common side-effect of bi-segment rectifiers [5,16,17]. However, compared with the proposals cited previously, our implementation is up-scaled in size to meet the requirements that fabrication and measure impose,

* Corresponding author at: Max Planck Institute for Polymer Research, Ackermannweg 10, 55128, Mainz, Germany.
E-mail address: graczykowski@mpip-mainz.mpg.de (B. Graczykowski).
[1] M.K. and M.S. contributed equally.

https://doi.org/10.1016/j.nanoen.2020.105261
Received 28 May 2020; Received in revised form 17 July 2020; Accepted 3 August 2020
Available online 8 August 2020
2211-2855/© 2020 The Authors. Published by Elsevier Ltd. This is an open access article under the CC BY license (http://creativecommons.org/licenses/by/4.0/).

and it operates at much higher temperatures. The tested devices are based on an alternative approach to the Joule effect based heater–thermometer platform [20–22], i.e. symmetric arrangement of two identical rectifiers. We use all-optical two-laser Raman thermometry (2LRT) [29,30] to induce the heat flow in the devices and provide the temperature distribution quantitatively. Furthermore, it does not require any modeling of the heat flow bypassing the rectifier or assumptions about the thermal resistance of the heater like in the electric heater–thermometer experiment. On the other hand, our approach is based on two test devices (forward and reverse heat flow directions); thus it requires a post-fabrication test of the samples' pattern identity. We show that our device can serve as a true thermal diode in moderate vacuum. In addition, we investigate the samples in air environment being relevant in terms of applications albeit not considered in prior studies. Although the symmetry of the samples cannot be guaranteed and hence rectification cannot be proved in this case, we propose potential applications such as air-triggered thermal switch or passive convective cooler. Finally, we provide extensive measurements of the thermal conductivity as a function of the temperature in spatially symmetric (or homogeneous) holey Si membranes. The extracted data has been used as input in Finite Element Method (FEM) simulations of the heat transport in spatially asymmetric (continuous inhomogeneous) systems, showing a good account of the non-reciprocal heat transport.

2. Materials and methods

2.1. Nanofabrication

All samples were fabricated on freestanding, single-crystal (001) silicon membranes with a thickness of 260 nm (Norcada Inc). When fabricating the thermal rectifier devices, all the attempts at using a standard electron beam lithography (EBL) and reactive ion etching (RIE) process resulted in serious damage to the membranes. Consequently, they were fabricated by a focused ion beam (FIB)-based method instead. Thus, a protective, 50-nm-thick Au layer was sputtered onto the membranes (EMS 150T Plus) to reduce the ion-induced damage [31]. The samples were patterned using a FIB (JEOL JIB-4000) equipped with Xenos XeDraw. The FIB milling process, employing gallium ions, was performed at an accelerated voltage of 30 kV. Holes were patterned with a dwell time of 49.5 μs per one pixel, a center-to-center pixel distance of 1 nm and ten repetitions. These parameter values provided an ion dose sufficient to perforate the silicon membrane. After removing the Au layer by selective etching (Sigma) for 1 h, the samples were rinsed in deionized water and ethanol.

The samples with homogeneous geometry were fabricated by EBL and RIE and using the Bosch process. The positive EBL resist AR-P 6200 (Allresist) was spun at 4000 rpm for 1 min and baked at 150 °C for 1 min. The EBL was performed at 30 kV (Raith 150-TWO). The pattern was transferred to silicon using the Bosch process (Alcatel AMS-110DE) at the following parameter values: source power (500 W); chuck power (15 W); SF_6 gas flow (150 sccm); and C_4F_8 gas flow (100 sccm). Finally, the samples were cleaned in an oxygen plasma system (PVA Tepla) at 400 W using an oxygen flow of 50 sccm for 10 min [30,32].

2.2. Two-laser Raman Thermometry (2LRT)

Our 2LRT setup employs two continuous-wave lasers: a high-powered one used as heater (λ = 405 nm) and a low-powered one used as temperature probe (λ = 532 nm). The heating beam is focused on the central portion of the sample through a long working distance microscope objective (Olympus 50×, NA = 0.55) and forms the Gaussian heat source on the non-perforated area of the membrane. The absorbed power P_A is measured by a calibrated system of three power meters (for incident, reflected and transmitted light) and a non-polarizing cube beam splitter. The error of P_A is about ΔP_A = 2%. The sample is mounted in the vacuum chamber (< 10^{-3} mbar) of a cryostat (Linkam THMS350V), which is attached to an xy-motorized stage. The probe beam at a power level less than 1% of P_A is focused onto the sample surface through the top-mounted microscope objective (Olympus 50×, NA = 0.55). The inelastically (Raman) backscattered light is directed to the spectrometer (T64000 Horiba). The spectral position ω_R of the longitudinal optical (LO) phonon of silicon was translated to temperature using the calibrated formula $T = 293\,\mathrm{K} + (\omega_0 - \omega_R)\cdot 43.43 \pm 0.05\,\mathrm{K/cm^{-1}}$, where ω_0 is the spectral position of LO phonon at T = 293 K. The temperature uncertainty of this method is typically lower than 3% [29,30,33].

3. Results and discussion

Following prior studies, we fabricated sub-micrometer holes in the silicon membranes, which provided a geometric means to achieve the temperature T and position r dependence of the thermal conductivity, $\kappa(T,r)$. The well-accepted explanation for this effect at high temperatures is the shortening of the phonon mean free path (MFP) due to phonon diffusive scattering at hole boundaries [30,34–40]. Currently, there is no consensus on which geometric parameter of porosity quantification could be correlated to $\kappa(T)$ being relevant for rectification [30,34–36,41–46]. However, in our work, we experimentally confirmed that the surface-to-volume ratio γ defined as the area of holes over the volume per the unit cell could serve as such a universal measure similarly as demonstrated for κ [47–49]. We designed the thermal rectifier as a free-standing bridge made of a crystalline silicon membrane (Fig. 1(a)). The structure is spatially asymmetric in terms of porosity, which gradually decreases from A to B. This non-regular arrangement is expected to introduce the necessary inhomogeneity to the system, i.e. an explicit dependence of the thermal conductivity on position. Two configurations of the rectifier subjected to thermal biases of the same magnitude, albeit in opposite directions (forward and reverse configurations), are displayed in Fig. 1(a). In both cases, the phonon MFPs are already shortened by phonon–phonon scattering processes near the hot ends and the holes have only a minor effect. Contrariwise, the porosity strongly influences the MFP near the cold ends. There, diffuse boundary scattering overwhelms the phonon–phonon processes, such that the MFPs in the reverse configuration are shorter than those in the forward one. Consequently, the two arrangements in Fig. 1(a) are unequal in terms of effective thermal conductivity. Specifically, the effective thermal conductivity of the forward configuration, κ_F, is higher than that of the reverse configuration, κ_R. Accordingly, we define the rectification coefficient as $\eta = (\kappa_F - \kappa_R)/\kappa_R$ [21]. Although our design is based on a single material, it can be considered topologically non-homogeneous given the engineered porosity gradient across its surface. The fact that the thermal conductivity κ of this system depends on temperature T and position r provides the conditions for rectification, i.e., material nonlinearity and spatial asymmetry, respectively.

To evaluate the thermal rectification, we designed an experiment using 2LRT technique [29,30,33] as schematically illustrated in Fig. 1(b). The probe laser is coupled to a Raman spectrometer and works as a scanning thermometer. Each test device comprises two identical rectifiers (in the forward configuration in Fig. 1(b)) arranged symmetrically with respect to the central neck. The latter is not perforated and serves as a focal point for the bottom, high-power laser (heat source). Heat flows symmetrically from the center towards the edges connected to the heat sink without exchange with any other reservoir. This configuration under vacuum conditions ensures thermal enclosure of the system, and hence insulation from reservoirs other than the heat sink. Therefore, the experiment approximates the ideal system model for rectification [Supplementary Material (SM) Figure S1]. Overall, the all-optical 2LRT allows for temperature scans and generation of temperature gradients up to about 1000 K.

We fabricated the thermal rectifier with a pseudo-hexagonal lattice of holes of constant diameter and varied spacing adjusted to obtain a linear gradient of γ along the rectifier axis. This approach provided a

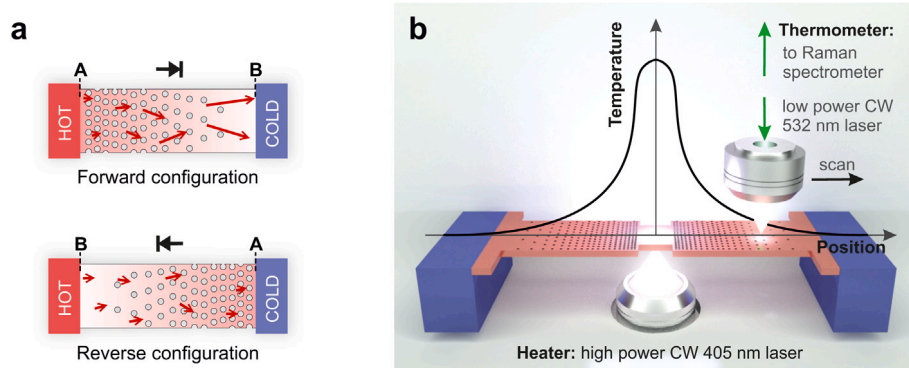

Fig. 1. Working principle and design of the thermal rectifier. (a) Design of the samples in the forward (top) and reverse (bottom) configurations. A and B indicate the ends of the rectifier, and the red arrows denote phonon mean free paths. (b) Schematic of the two-laser Raman thermometry experiment, running in the forward configuration of the test device. The high-power beam (405 nm) is focused from the bottom on the central neck of the sample, gets partially absorbed and acts as a Gaussian heat source. The low-power laser beam (532 nm), focused from the top, is coupled to a Raman spectrometer and works as a scanning thermometer.

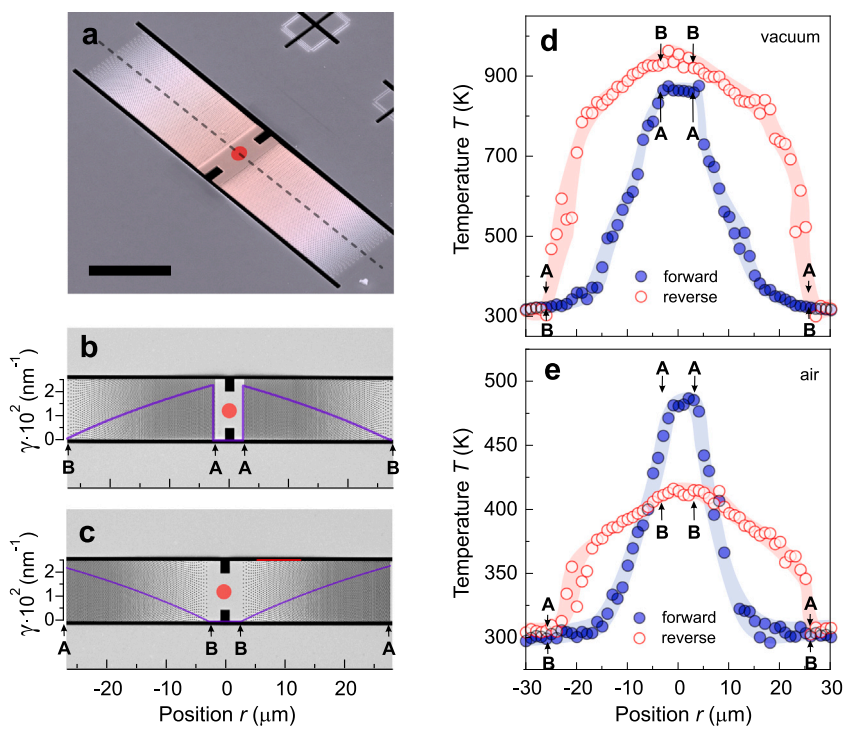

Fig. 2. Thermal rectifier test devices. (a) Scanning electron microscope image of the test device comprising two rectifiers assembled in the forward configuration. The red dot indicates the heat source and the dashed line indicates the temperature scan line. Scale bar is 10 μm. (b, c) Scanning electron microscope images (top view) of the test devices in (b) the forward and (c) reverse configurations. Overlay of the images in (b) and (c) illustrates spatial dependence of the surface-to-volume ratio γ. (d, e) Plots of the temperature profiles of the test devices in the forward (solid purple circles) and reverse (red-outlined circles) configurations, as measured at P_A = 0.815 mW in (d) vacuum or (e) in air at ambient pressure. The pale red and purple shading in (d) and (e) correlate to the eye-covering experimental errors (see SM).

medium with effective thermal conductivity $\kappa(T, r)$, which is not a separable function of temperature T and position r, therefore satisfying the necessary condition for rectification. A scanning electron microscope (SEM) image of the test device comprising two rectifiers assembled in the forward configuration is shown in Fig. 2(a).

Figs. 2(b) and 2(c) show SEM images of the test devices in the forward and reverse configurations, respectively, with overlays depicting the experimental $\gamma(r)$ (Figure S9). In both experimental configurations, we use the same heat flux, which we obtained by setting the same driving power $P = P_A/2$, where P_A is the absorbed laser power (see also Figure S1). This approach is more convenient than setting the same temperature bias for both configurations, since using 2LRT enables more accurate matching of P_A. Consequently, the rectification coefficient transforms into $\eta = \Delta T_{BA}/\Delta T_{AB} - 1$, where $\Delta T_{BA} = T_B - T_A$ and $\Delta T_{AB} = T_A - T_B$.

Fig. 2(d) reveals a clear difference between the temperature profiles $T(r)$ obtained for the two configurations of the test devices operating in vacuum. Interestingly, the reverse configuration shows a greater temperature bias than does the forward one. Accordingly, $\Delta T_{BA} > \Delta T_{AB}$ and therefore, $\eta > 0$, which indicates asymmetric heat transport. Despite of their different thermal profiles (see Fig. 2(e)), the symmetry between the two sample configurations cannot be guaranteed and hence rectification cannot be asserted when measurements are performed in air (Figures S3 and S4 in SM) [7,50]. Nevertheless, we will further discuss two potential applications of the devices exploiting air convection.

Fig. 3(a) summarizes 2LRT measurements at diverse heating powers in the form of transfer functions $\Delta T(P)$ resembling the voltage–current characteristics in electronics. Importantly, we observe asymmetry in the

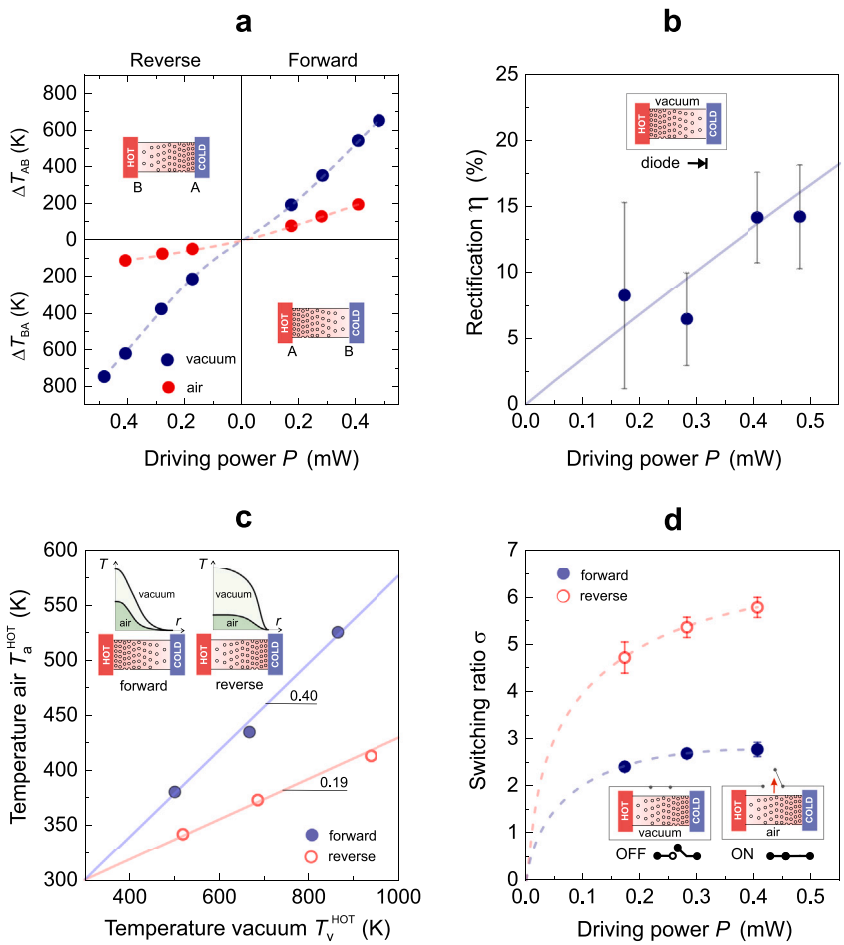

Fig. 3. Performance of the test devices. (a) Transfer functions of the rectifier measured in vacuum and in air at ambient pressure. (b) Rectification coefficient η as a function of the driving power P measured in vacuum. The solid line in (b) denotes rectification calculated by means of Finite Element Method model (SM). The error propagation is described in SM. (c) Temperature measured at the hot end of the sample in vacuum (T_v^{HOT}) and in air (T_a^{HOT}) in two configurations of the device. The islet to (c) illustrates the difference between the configurations in terms of air-mediated heat losses. (d) Plot of the on/off (air/vacuum) switching ratio σ as a function of P, as determined for the forward and reverse configurations. The dashed lines in (a, d) are guides to the eye. The error propagation is described in SM.

transfer functions for our samples operating in vacuum as well as in air. However, only the measurements performed in vacuum hold the proper symmetry. In this case, the system can be considered as a true thermal diode (Figures S1 and S2 in SM). Fig. 3(b) shows the experimental η as a function of the driving power P. For the sample in vacuum, η increases with P, reaching maximum performance ($\eta \cong 14\%$) at $P \cong 0.5$ mW. This trend is well reproduced by FEM simulations (S5 in the SM). The performance could be further improved through optimization of structural parameters such as the membrane patterning or thickness (see FEM results in Figs. S18 and S20 in SM).

The data in Fig. 3(a) obtained in air reveals effective switching of the configurations, namely $\Delta T_{BA} < \Delta T_{AB}$. Furthermore, exposure to air results in a decrease of the temperature along $T(r)$, as evidenced by comparing Fig. 2(d) and Fig. 2(e). This effect can be quantified by comparing temperatures measured at the hot end of the sample in vacuum (T_v^{HOT}) and in air (T_a^{HOT}). From Fig. 3(c) we conclude that the temperature in air reduces of about 60% and 81% in the case of forward and reverse configurations, respectively. This apparent difference can be explained by analogy to the ideal case of a fin heat sink, whereby a fin performs best when the temperature distribution over its entire surface is uniform [51]. As evidenced in Fig. 2(e) and schematically illustrated in the inset to Fig. 3(c), the temperature profile for the reverse configuration of the test device is closer to this scenario. In the case of the forward configuration, heat flows first through the part of high porosity, which translates to a lower thermal conductance due to both reduced κ and effective cross section. This bottleneck implies smaller dissipation through a secondary mechanism, i.e. convection [52]. The local convective heat flux is proportional to the temperature difference between sample surface and air. This temperature difference rapidly decays due to the high porosity region near the hot spot in the forward case. Importantly, engineering the porosity to optimize passive cooling is not trivial, as the material thermal properties depend on size as well as geometry. The device in air environment has the potential to be used as a passive cooler for efficient removal of redundant process heat in Si membrane-based electronics, micro- and nano-electromechanical systems or optomechanics.

Moreover, we envisioned that the significant difference in transfer functions between the samples in vacuum and those in air (Fig. 3(a)) could be exploited in the design of an air-triggered thermal switch. The performance of such a device is indicated by the on/off switching ratio $\sigma = \Delta T_v / \Delta T_a$, where ΔT_v and ΔT_a are the temperature biases induced by the same power and in the same configuration in vacuum and in air, respectively. As shown in Fig. 3(d), we observed clearly defined on/off states for both configurations at any driving power.

To confirm the working principle and rationalize the measured performance of our thermal diode, we next examined $\kappa(T)$ of silicon membranes of homogeneous porosity. To this end, we fabricated a set of porous, single-crystal silicon membranes and patterned them with a

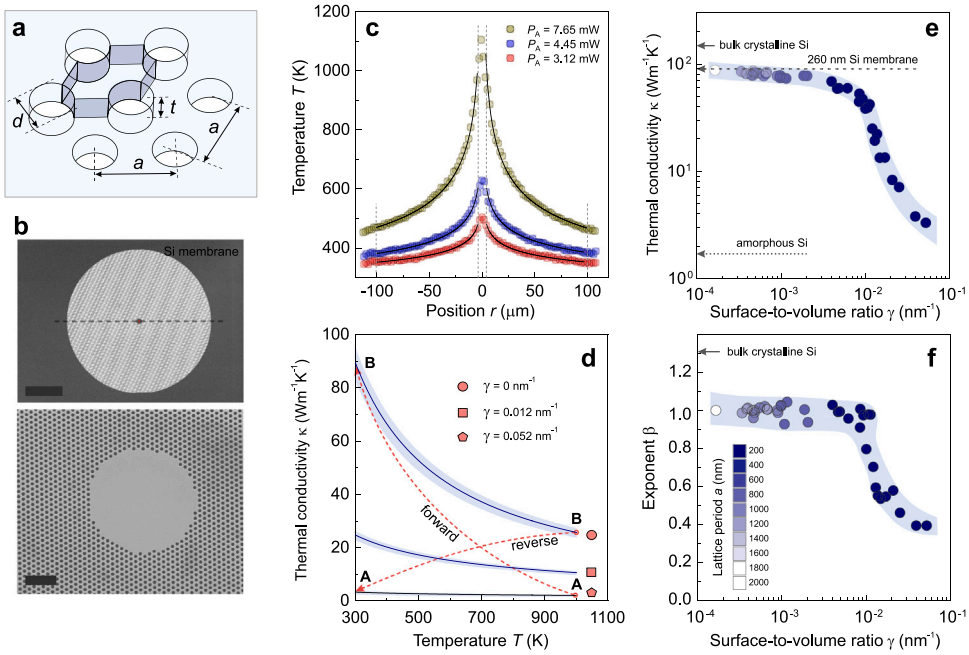

Fig. 4. Thermal conductivity of homogeneous porous membranes. (a) Schematic of the hexagonal lattice of holes in a silicon membrane with a marked unit cell. Here, t denotes membrane thickness; d, hole diameter; and a, lattice period. (b) Scanning electron microscope images of a porous sample: top-view (top) and magnified central area (bottom). The dashed line indicates the temperature scan line. Scale bars are 50 μm (top) and 2 μm (bottom). (c) Measured (circles), and fitted by Eq. (1) (lines), temperature profile plots obtained for a porous membrane of a=800 nm and d=192 nm (γ=0.0012 nm^{-1}), at three different heating powers P_A. The vertical dashed lines indicate the edges of the porous area. (d) Plot of temperature dependence of thermal conductivity (solid lines) determined for porous membranes of exemplary surface-to-volume ratio γ. (e) Thermal conductivity of porous membranes at 300 K as a function of γ. (f) Plot of exponent β of porous membranes as a function of γ. The shaded areas in (d–f) indicate experimental uncertainty (SM).

regular arrangement in the form of an hexagonal lattice of cylindrical holes. We measured their $\kappa(T)$ by 2LRT in vacuum assuming that the convective and radiative losses are both negligible (see SM). Fig. 4(a) illustrates the lattice unit-cell, where a is the lattice parameter and d is the pore/hole diameter. We covered a broad range of γ values by varying a (from 200 nm to 2000 nm) and d (from 55 nm to 190 nm). Fig. 4(b) shows SEM images of a representative sample. Fig. 4(c) displays temperature profiles $T(r)$ measured for a sample of a = 800 nm and d = 192 nm, where r is the distance from the central heat source. We performed 2LRT experiments at three values of absorbed power P_A; thus, the temperature profiles being partially overlapped span temperatures from about 350 K to 1000 K. We considered the heat flow to be diffusive and radial, and thus described by Fourier's law: $P_A/(2\pi rt) = -\kappa(T)\mathrm{d}T/\mathrm{d}r$ [30]. At high temperatures, the $\kappa(T)$ of bulk silicon is governed by three- and four-phonon scattering processes [53] and can be approximated by the power function $\kappa(T) = \alpha T^{(-\beta)}$ [54]. Following prior studies on homogeneous porous graphene [14,55] and silicon [30,56], we assumed that the same trend holds for our samples in the full range of γ values. The additional effect of diffusive phonon-boundary scattering is temperature-independent at high temperatures and can be included by adjusting α and β.

Accordingly, the decrease of β reflects the suppression of the temperature dependence of κ due to porosity. Substituting the postulated $\kappa(T)$ into Fourier's law, we obtained after integration:

$$T = \left(A - \frac{P_A(1-\beta)}{2\pi t\alpha}\ln|r|\right)^{1/(1-\beta)}, \quad (1)$$

where A is an integration constant. This formula enables adjusting α and β from the fit to the experimental temperature profiles, as shown in Fig. 4(c). To obtain the intrinsic $\kappa(T)$, we normalized the fitted data using the correction factor ε, accounting for the porosity of the hexagonal lattice (see SM). Fig. 4(d) shows $\kappa(T)$ determined for three samples with representative values of γ, ranging from γ = 0 (for a pristine membrane) up to γ = 0.0052 nm^{-1} (the maximum value of the full set). Fig. 4(d) confirms that with increasing γ, κ becomes suppressed and $\kappa(T)$ flattens. This behavior is generalized for all γ in Figs. 4(e) and 4(f). From Fig. 4(e), we inferred that at T=300 K, κ decreases systematically, from ≈ 90 W m^{-1}K^{-1} for the pristine membrane to ≈ 3.3 W m^{-1}K^{-1} at maximum γ. Fig. 4(f) depicts a clear trend of β gradually decreasing from ≈ 1 (for a bare membrane) to ≈ 0.4 (for the most porous sample) owing to the increased and predominant boundary scattering.

In Fig. 4(d), the two dashed arrows connecting A and B indicate hypothetical paths through intermediate states of κ that correspond to the forward and reverse configurations shown in Fig. 1(a). These intermediate values of κ can be assumed as the local thermal conductivity of an hypothetical sample with γ varying linearly with r. Therefore, the local thermal conductivity at any position $r = r_0$ is taken as the value of κ of a sample with homogeneous $\gamma = \gamma(r_0)$ and at the temperature $T = T(r_0)$. We notice that these two cases are unequal, namely, that relative to the path A–B, the path B–A covers mostly lower values of κ. Consequently, heat transport from A to B (forward) is easier than from B to A (reverse). Notably, the rectification coefficient calculated by means of FEM (Fig. 3(b)) using measured values for α and β closely agrees with the experimental data. The dependence of κ on temperature and surface-to-volume ratio is essential for rectification. Namely, rectification is forbidden for any asymmetric single-component material when its thermal conductivity κ is a separable function of the position r and temperature T [57]. This can be formulated as $\kappa(r,T) = X(r)\cdot\Theta(T)$, where $X(r)$ and $\Theta(T)$ depend only on position and temperature, respectively. In our case, the necessary condition is fulfilled, as the thermal conductivity is provided by the function $\kappa(r,T) = \alpha(r)\cdot T^{-\beta(r)}$.

4. Conclusions

We have designed, fabricated and tested a thermal rectifier comprising porous crystalline silicon membranes, where reciprocity is broken

as a result of non-linearity and space asymmetry. It can operate as a thermal diode at temperatures ranging from 300 K to about 1000 K at sub-milliwatt powers in vacuum. We have achieved the best rectification coefficient for an all-silicon device, i.e. a continuous inhomogeneous medium without a distinct interface working in a high temperature environment. We have further demonstrated that the same device can work under air pressure as an air-triggered switch or a passive cooler. Moreover, we have provided a complete account of the $\kappa(T)$ dependence in a wide range of porosity values. We have showed that using these values as input values of the position and temperature dependent thermal conductivity in a FEM simulation of the diffusive heat transport, the model gives a good account of the rectification. Therefore, it can be used as a convenient tool for further optimization of the rectifier performance or the design of other elements and devices for heat transport control. These results are of much relevance to a variety of applications embracing thermal energy management and harvesting, thermal logics, all merged into a single CMOS-compatible platform. They can trigger new strategies of heat dissipation and passive cooling in electronics and MEMS operating at environmental conditions involving high temperatures and high temperature gradients. The approach can be extended from Si and SOI materials to the alike Ge and GaAs, but also the new generation of wide band-gap materials like SiC and GaN suited for electronics and MEMS operating at extremely high temperatures.

CRediT authorship contribution statement

Maciej Kasprzak: Fabricated samples, Wrote the manuscript, Performed experiments, Discussion, Interpretation of the results. **Marianna Sledzinska:** Fabricated samples, Wrote the manuscript, Performed experiments, Discussion, Interpretation of the results. **Karol Zaleski:** Fabricated samples, Discussion, Interpretation of the results. **Igor Iatsunskyi:** Fabricated samples, Discussion, Interpretation of the results. **Francesc Alzina:** Wrote the manuscript, Discussion, Interpretation of the results. **Sebastian Volz:** Discussion, Interpretation of the results. **Clivia M. Sotomayor Torres:** Discussion, Interpretation of the results. **Bartlomiej Graczykowski:** Identified the research topic, Wrote the manuscript, Performed experiments, Discussion, Interpretation of the results.

Declaration of competing interest

The authors declare that they have no known competing financial interests or personal relationships that could have appeared to influence the work reported in this paper.

Acknowledgments

The work was supported by Polish National Science Centre (Sonata UMO-2018/31/D/ST3/03882 and Preludium UMO-2019/33/N/ST5/02902). B.G. acknowledge the support from the Foundation for Polish Science (POIR.04.04.00-00-5D1B/18). The ICN2 is funded by the CERCA programme/Generalitat de Catalunya. The ICN2 is supported by the Severo Ochoa Centres of Excellence programme, funded by the Spanish Research Agency (AEI, grant no. SEV-2017-0706). M.S., F.A. and C.M.S.T. acknowledge support from Spanish MICINN project SIP (PGC2018-101743-B-I00).

Appendix A. Supplementary data

Non-Reciprocity/ Time-reversal symmetry breaking/ Asymmetric propagation. Sample preparation. Thermal conductivity of porous membranes. Thermal rectification. Finite Element Method modelling.

Supplementary material related to this article can be found online at https://doi.org/10.1016/j.nanoen.2020.105261.

References

[1] J.D. Cressler, H.A. Mantooth, Extreme Environment Electronics, CRC Press.
[2] A. Sharif, Harsh Environment Electronics: Interconnect Materials and Performance Assessment, John Wiley & Sons.
[3] J.-P. Colinge, Silicon-on-Insulator Technology: Materials to VLSI, second ed., Springer US.
[4] B. Li, L. Wang, G. Casati, Thermal diode: Rectification of heat flux, Phys. Rev. Lett. 93 (18) (2004) 184301.
[5] G. Wehmeyer, T. Yabuki, C. Monachon, J. Wu, C. Dames, Thermal diodes, regulators, and switches: Physical mechanisms and potential applications, Appl. Phys. Rev. 4 (4) (2017) 041304.
[6] C.W. Chang, D. Okawa, A. Majumdar, A. Zettl, Solid-state thermal rectifier, Science 314 (5802) (2006) 1121–1124.
[7] A. Maznev, A. Every, O. Wright, Reciprocity in reflection and transmission: What is a phonon diode? Wave Motion 50 (4) (2013) 776–784.
[8] N.A. Roberts, D. Walker, A review of thermal rectification observations and models in solid materials, Int. J. Therm. Sci. 50 (5) (2011) 648–662.
[9] M.J. Martínez-Pérez, A. Fornieri, F. Giazotto, Rectification of electronic heat current by a hybrid thermal diode, Nature Nanotechnol. 10 (4) (2015) 303.
[10] H. Hoff, Asymmetrical heat conduction in inhomogeneous materials, Physica A 131 (2) (1985) 449–464.
[11] N. Yang, N. Li, L. Wang, B. Li, Thermal rectification and negative differential thermal resistance in lattices with mass gradient, Phys. Rev. B 76 (2) (2007) 020301.
[12] C. Dames, Solid-state thermal rectification with existing bulk materials, J. Heat Transfer 131 (6) (2009) 061301, http://dx.doi.org/10.1115/1.3089552.
[13] X. Cartoixà, L. Colombo, R. Rurali, Thermal rectification by design in telescopic si nanowires, Nano Lett. 15 (12) (2015) 8255–8259.
[14] Y. Wang, A. Vallabhaneni, J. Hu, B. Qiu, Y.P. Chen, X. Ruan, Phonon lateral confinement enables thermal rectification in asymmetric single-material nanostructures, Nano Lett. 14 (2) (2014) 592–596.
[15] T. Zhang, T. Luo, Giant thermal rectification from polyethylene nanofiber thermal diodes, Small 11 (36) (2015) 4657–4665.
[16] R. Dettori, C. Melis, R. Rurali, L. Colombo, Thermal rectification in silicon by a graded distribution of defects, J. Appl. Phys. 119 (21) (2016) 215102.
[17] H. Machrafi, Extended Non-Equilibrium Thermodynamics: from Principles to Applications in Nanosystems, CRC Press, 2019.
[18] X.K. Chen, M. Pang, T. Chen, D. Du, K.-Q. Chen, Thermal rectification in asymmetric graphene/hexagonal boron nitride van der Waals heterostructures, ACS Appl. Mater. Interfaces (2020).
[19] W. Kobayashi, Y. Teraoka, I. Terasaki, An oxide thermal rectifier, Appl. Phys. Lett. 95 (17) (2009) 171905.
[20] H. Tian, D. Xie, Y. Yang, T.-L. Ren, G. Zhang, Y.-F. Wang, C.-J. Zhou, P.-G. Peng, L.-G. Wang, L.-T. Liu, A novel solid-state thermal rectifier based on reduced graphene oxide, Sci. Rep. 2 (1) (2012) 1–7.
[21] H. Wang, S. Hu, K. Takahashi, X. Zhang, H. Takamatsu, J. Chen, Experimental study of thermal rectification in suspended monolayer graphene, Nat. Commun. 8 (1) (2017) 1–8.
[22] H.S. Choe, R. Prabhakar, G. Wehmeyer, F.I. Allen, W. Lee, L. Jin, Y. Li, P. Yang, C.-W. Qiu, C. Dames, et al., Ion write microthermotics: Programing thermal metamaterials at the microscale, Nano Lett. 19 (6) (2019) 3830–3837.
[23] M. Schmotz, J. Maier, E. Scheer, P. Leiderer, A thermal diode using phonon rectification, New J. Phys. 13 (11) (2011) 113027.
[24] S. Gluchko, R. Anufriev, R. Yanagisawa, S. Volz, M. Nomura, On the reduction and rectification of thermal conduction using phononic crystals with pacman-shaped holes, Appl. Phys. Lett. 114 (2) (2019) 023102.
[25] Z. Chen, C. Wong, S. Lubner, S. Yee, J. Miller, W. Jang, C. Hardin, A. Fong, J.E. Garay, C. Dames, Retraction: A Photon Thermal Diode, Nature Publishing Group, 2017.
[26] B.V. Budaev, Correspondence: The experimental requirements for a photon thermal diode, Nat. Commun. 8 (1) (2017) 1–2.
[27] S. Hu, M. An, N. Yang, B. Li, A series circuit of thermal rectifiers: an effective way to enhance rectification ratio, Small 13 (6) (2017) 1602726.
[28] M. Criado-Sancho, F. Alvarez, D. Jou, Thermal rectification in inhomogeneous nanoporous Si devices, J. Appl. Phys. 114 (5) (2013) 053512.
[29] J. Reparaz, E. Chavez-Angel, M. Wagner, B. Graczykowski, J. Gomis-Bresco, F. Alzina, C. Sotomayor Torres, A novel contactless technique for thermal field mapping and thermal conductivity determination: two-laser Raman thermometry, Rev. Sci. Instrum. 85 (3) (2014) 034901.
[30] B. Graczykowski, A. El Sachat, J.S. Reparaz, M. Sledzinska, M.R. Wagner, E. Chavez-Angel, Y. Wu, S. Volz, F. Alzina, C.S. Torres, Thermal conductivity and air-mediated losses in periodic porous silicon membranes at high temperatures, Nat. Commun. 8 (1) (2017) 1–9.

[31] S. Rubanov, P. Munroe, The effect of the gold sputter-coated films in minimising damage in FIB-produced TEM specimens, Mater. Lett. 57 (15) (2003) 2238–2241.

[32] M. Sledzinska, B. Graczykowski, F. Alzina, J.S. Lopez, C.S. Torres, Fabrication of phononic crystals on free-standing silicon membranes, Microelectron. Eng. 149 (2016) 41–45.

[33] M.R. Wagner, B. Graczykowski, J.S. Reparaz, A. El Sachat, M. Sledzinska, F. Alzina, C.M. Sotomayor Torres, Two-dimensional phononic crystals: Disorder matters, Nano Lett. 16 (9) (2016) 5661–5668.

[34] J.-K. Yu, S. Mitrovic, D. Tham, J. Varghese, J.R. Heath, Reduction of thermal conductivity in phononic nanomesh structures, Nature Nanotechnol. 5 (10) (2010) 718–721.

[35] J. Lee, W. Lee, G. Wehmeyer, S. Dhuey, D.L. Olynick, S. Cabrini, C. Dames, J.J. Urban, P. Yang, Investigation of phonon coherence and backscattering using silicon nanomeshes, Nat. Commun. 8 (1) (2017) 1–8.

[36] J. Maire, R. Anufriev, R. Yanagisawa, A. Ramiere, S. Volz, M. Nomura, Heat conduction tuning by wave nature of phonons, Sci. Adv. 3 (8) (2017) e1700027.

[37] M. Maldovan, Sound and heat revolutions in phononics, Nature 503 (7475) (2013) 209–217.

[38] M. Maldovan, Phonon wave interference and thermal bandgap materials, Nat. Mater. 14 (7) (2015) 667–674.

[39] K. Takahashi, M. Fujikane, Y. Liao, M. Kashiwagi, T. Kawasaki, N. Tambo, S. Ju, Y. Naito, J. Shiomi, Elastic inhomogeneity and anomalous thermal transport in ultrafine si phononic crystals, Nano Energy 71 (2020) 104581.

[40] M. Haras, T. Skotnicki, Thermoelectricity for IoT–A review, Nano Energy 54 (2018) 461–476.

[41] J. Lim, H.-T. Wang, J. Tang, S.C. Andrews, H. So, J. Lee, D.H. Lee, T.P. Russell, P. Yang, Simultaneous thermoelectric property measurement and incoherent phonon transport in holey silicon, ACS Nano 10 (1) (2016) 124–132.

[42] P. Martin, Z. Aksamija, E. Pop, U. Ravaioli, Impact of phonon-surface roughness scattering on thermal conductivity of thin Si nanowires, Phys. Rev. Lett. 102 (2009) 125503.

[43] A. Jain, Y.-J. Yu, A.J.H. McGaughey, Phonon transport in periodic silicon nanoporous films with feature sizes greater than 100 nm, Phys. Rev. B 87 (2013) 195301, http://dx.doi.org/10.1103/PhysRevB.87.195301.

[44] P.E. Hopkins, C.M. Reinke, M.F. Su, R.H. Olsson III, E.A. Shaner, Z.C. Leseman, J.R. Serrano, L.M. Phinney, I. El-Kady, Reduction in the thermal conductivity of single crystalline silicon by phononic crystal patterning, Nano Lett. 11 (1) (2011) 107–112.

[45] J. Tang, H.-T. Wang, D.H. Lee, M. Fardy, Z. Huo, T.P. Russell, P. Yang, Holey silicon as an efficient thermoelectric material, Nano Lett. 10 (10) (2010) 4279–4283.

[46] M. Sledzinska, B. Graczykowski, J. Maire, E. Chavez-Angel, C.M. Sotomayor-Torres, F. Alzina, 2d phononic crystals: Progress and prospects in hypersound and thermal transport engineering, Adv. Funct. Mater. (2019) 1904434.

[47] R. Dettori, C. Melis, X. Cartoixa, R. Rurali, L. Colombo, Model for thermal conductivity in nanoporous silicon from atomistic simulations, Phys. Rev. B 91 (5) (2015) 054305.

[48] M. Verdier, R. Anufriev, A. Ramiere, K. Termentzidis, D. Lacroix, Thermal conductivity of phononic membranes with aligned and staggered lattices of holes at room and low temperatures, Phys. Rev. B 95 (20) (2017) 205438.

[49] R. Anufriev, J. Maire, M. Nomura, Reduction of thermal conductivity by surface scattering of phonons in periodic silicon nanostructures, Phys. Rev. B 93 (4) (2016) 045411.

[50] C. Caloz, A. Alù, S. Tretyakov, D. Sounas, K. Achouri, Z.-L. Deck-Léger, Electromagnetic nonreciprocity, Phys. Rev. A 10 (4) (2018) 047001.

[51] T.L. Bergman, F.P. Incropera, A.S. Lavine, D.P. DeWitt, Introduction to Heat Transfer, John Wiley & Sons, 2011.

[52] C. Cheng, W. Fan, J. Cao, S.-G. Ryu, J. Ji, C.P. Grigoropoulos, J. Wu, Heat transfer across the interface between nanoscale solids and gas, ACS Nano 5 (12) (2011) 10102–10107.

[53] T. Feng, L. Lindsay, X. Ruan, Four-phonon scattering significantly reduces intrinsic thermal conductivity of solids, Phys. Rev. B 96 (16) (2017) 161201.

[54] C. Glassbrenner, G.A. Slack, Thermal conductivity of silicon and germanium from 3 k to the melting point, Phys. Rev. 134 (4A) (1964) A1058.

[55] S. Hu, J. Chen, N. Yang, B. Li, Thermal transport in graphene with defect and doping: phonon modes analysis, Carbon 116 (2017) 139–144.

[56] D. Song, G. Chen, Thermal conductivity of periodic microporous silicon films, Appl. Phys. Lett. 84 (5) (2004) 687–689.

[57] D.B. Go, M. Sen, On the condition for thermal rectification using bulk materials, J. Heat Transfer 132 (12) (2010) 124502, http://dx.doi.org/10.1115/1.4002286.

Maciej Kasprzak received his M.Sc. in Physics in 2016 at the Faculty of Physics of Adam Mickiewicz University in Poznan, Poland. Currently he is a Ph.D. candidate and his research interests include nanoscale heat transfer and GPU computing.

Marianna Sledzinska received Ph.D. in Physics from Universitat Autonoma de Barcelona in 2012. Her research interests cover fabrication of 2D nanostructures and photonic/phononic crystals, structural and optical characterization, and thermal and electrical transport on the nanoscale.

Karol Zaleski received his Ph.D. degree in physics from Institute of Molecular Physics, Polish Academy of Sciences, Poznan. His Ph.D. research topic was development of magnetic shape memory thin films of Heusler Alloys. He is currently an adjunct at NanoBioMedical Centre, Adam Mickiewicz University, Poznan, Poland. Recently, his research interests include study of materials for 2D spintronic devices.

Igor Iatsunskyi obtained a Master degree in physics, Faculty of Physics, Odessa National I.I. Mechnikov University in 2005. In 2009 he has obtained Ph.D. degree in Physics and in 2019 Habilitation degree in Materials Science at AHG University of Science and Technology (Poland). His current position is an Associate Professor at NanoBioMedical Centre (Adam Mickiewicz University), Poznan, Poland. His scientific interests are metal oxides nanostructures, organic semiconductors and hybrid structures for sensors, optical fiber sensors, semiconductor and surface physics, biosensors and medical applications.

Francesc Alzina is a senior researcher at the Catalan Institute of Nanoscience and Nanotechnology (ICN2). After receiving his Ph.D. from the Universitat Autonoma de Barcelona, he was appointed as postdoctoral researcher at the National Renewable Energy Laboratory (NREL) in USA and, later, at the Paul Drude Institute in Germany. He joined the Phononic and Photonic Nanostructures Group in 2011 and, since then, he has been performing research on the phonon-related properties of low dimensional and nanostructured materials, with interests spanning from control of phonon propagation and confinement in phononic crystals and cavities to thermal transport by phonons.

Sebastian Volz obtained Ph.D. in Mechanical Engineering in 1996 (U. Poitiers, France). During 1997–1998 he was a postdoctoral research assistant at UCLA. He held tenured positions as: 1998–2000 Assistant Professor in Heat Transfer, ENSMA; 2001–2008 CNRS Research Fellow at Ecole Centrale Paris; 2009–2010 CNRS Senior Research Fellow at University of Tokyo; 2010–2016 CNRS Senior Research Fellow at Ecole Centrale Paris where he led the Thermal Nanosciences group. Currently he is the director of the international laboratory LIMMS in Tokyo. He carries out research in solid state nanoscale thermal transport, including phonon–electron–photon modeling and metrologies for key applications such as thermoelectricity, photovoltaics and IC cooling.

Clivia M. Sotomayor Torres obtained her Ph.D. in Physics (Manchester Univ., UK 1984). She held tenured appointments at St. Andrews and Glasgow Universities and became a C4 professor at Wuppertal Univ. (Germany 1996). During 2004–8 she was a research professor at Univ. College Cork, Tyndall National Institute (Ireland). Since 2007 she is at ICN2 and heads a team working on phonon engineering and nanofabrication. Clivia received awards from the Royal Society of Edinburgh, the Nuffield Foundation and an Amelia Earhart Fellowship from ZONTA International (USA). She edited six books on low dimensional structures and nanofabrication. Recently she was awarded an ERC Advanced Grant.

Bartlomiej Graczykowski obtained his Ph.D. in Physics in 2012 (AMU, Poznan, Poland). He was appointed as a postdoctoral researcher at ICN2 Barcelona in Spain (2013–2016) and MPIP Mainz in Germany (A. von Humboldt Foundation fellowship, 2016–2017). Currently he is an assistant professor at the Faculty of Physics of Adam Mickiewicz University in Poznan, Poland and guest researcher at the Max Planck Institute for Polymer Research in Mainz, Germany. His research activities include advanced inelastic light scattering techniques (Brillouin, Raman) applied to nanostructures, hypersound and heat transport at the nanoscale in confined and organized systems.